# Conformational biosensors delineate endosomal G protein regulation by GPCRs

Brian Wysolmerski[1,2], Emily E. Blythe[1], Mark von Zastrow[1,3*]

[1]Department of Psychiatry and Behavioral Sciences, University of California, San Francisco, San Francisco CA, USA.
[2]Tetrad Graduate Program, University of California, San Francisco, San Francisco CA, USA.
[3]Department of Cellular and Molecular Pharmacology, University of California, San Francisco, San Francisco CA, USA
*Correspondence: mark.vonzastrow@ucsf.edu

## Abstract

Many GPCRs trigger a second phase of G protein-coupled signaling from endosomes after initiating signaling from the plasma membrane. This inherently requires receptors to increase the concentration of active-state G proteins on the endosome membrane, but how this is achieved remains incompletely understood. We addressed this question by dissecting the regulation of G protein abundance and activity on endosomes following activation of several $G_s$-coupled GPCRs–the β2-adrenergic receptor, the VIP-1 receptor, and the adenosine 2b receptor–that are natively co-expressed and differ in their ability to internalize after activation. We first verify GPCR-triggered redistribution of $G\alpha_s$ from the plasma membrane to a mixed population of intracellular membranes, including endosomes, that is both reversible after receptor inactivation and triggered irrespective of the ability of the GPCR to internalize. We next show that GPCRs trigger this redistribution process at native expression levels and describe a method, using conformational biosensors, to detect endosomal activation of endogenous $G\alpha_s$. Applying this method, we show that GPCR-mediated production of active-state $G\alpha_s$ on endosomes depends on receptor endocytosis, whereas increasing the net amount of $G\alpha_s$ on endosomes does not. Our results support a model for $G_s$ regulation on endosomes mediated by two spatially separated receptor coupling events–one at the plasma membrane controlling endosomal $G_s$ abundance and another at endosomes controlling $G_s$ activity. Additionally, our results reveal location-bias in the selectivity of G protein activation on endosomes that is differentially programmed by GPCRs in a receptor-specific manner.

## Introduction

G protein-coupled receptors (GPCRs) constitute the largest family of signaling receptors that regulate nearly every physiological process. After activation by binding an agonist, GPCRs initiate signaling by coupling to cognate heterotrimeric G proteins, consisting of a Gα subunit and Gβγ subcomplex, which function as key transducers of downstream signaling. This allosteric coupling reaction promotes guanine nucleotide exchange on the G protein α-subunit, resulting in GTP binding to the α-subunit that converts it from an inactive to active state. G protein classes are defined according to the identity of their α-subunit (e.g. $G_{s/olf}$, $G_{i/o}$, $G_{q/11}$, and $G_{12/13}$), with individual GPCRs differing in selectivity for coupling among G protein classes, and each class producing distinct downstream regulatory effects[1,2]. The central importance of GPCR signaling in physiology, and its dysfunction or dysregulation in pathological states, has motivated intense interest in GPCRs as therapeutic targets, with over 30% of presently FDA-approved drugs targeting GPCRs[3].

The importance of GPCR signaling from the plasma membrane has been recognized for many years[1,4], and there is now considerable interest in the ability of GPCRs to produce distinct and additional effects from intracellular membranes[4,5]. Endomembrane signaling is perhaps most strongly supported from the study of $G_s$-coupled GPCRs[4–16], but there is also significant evidence for endomembrane signaling through other G protein classes[5,17,18]. Such signaling fundamentally depends on the activated GPCR increasing the concentration of active-state G proteins on the appropriate membrane. When compared to the present knowledge about the subcellular localization of activated GPCRs, however, relatively little is known about how active-state G protein concentration on endomembranes is controlled.

$G_s$ is enriched on the plasma membrane and present in lower amounts on intracellular membranes[19]. $G_s$ activation by coupling to a GPCR on the plasma membrane promotes dissociation of $G\alpha_s$ and its net intracellular redistribution, increasing the concentration of $G\alpha_s$ on multiple endomembrane compartments, including endosomes[19–23]. Producing active-state

$G\alpha_s$ on endosomes is then thought to require a second coupling reaction locally on endosomes[4,5,9]. However, the presence of active-state $G\alpha_s$ on endosomes has only been hypothesized, and the cellular basis of the regulation of $G\alpha_s$ abundance and activity on endosomes remains unclear.

We addressed this knowledge gap by dissecting the regulation of endosomal $G\alpha_s$ abundance and activity by GPCRs that are natively co-expressed and significantly differ in their ability to internalize after activation. We first verify that GPCRs trigger a net intracellular redistribution of $G\alpha_s$ from the plasma membrane[19,20,22–24], and we then extend the present understanding by showing that this process is triggered by multiple $G_s$-coupled GPCRs and occurs under conditions of native or near-native levels of GPCR and $G\alpha_s$ expression. Next, using conformational biosensors, we demonstrate sequential phases of both $G_s$ activation and of active-state $G\alpha_s$ accumulation, first on the plasma membrane and then endosomes, at endogenous levels of G protein expression. We then show that $G_s$ activation on endosomes is specifically dependent on receptor endocytosis. Finally, we provide evidence for a type of 'location bias' in the biochemical selectivity of endosomal G protein activation that is differentially programmed by GPCRs in a remarkably receptor-specific manner.

## Results

### *$G\alpha_s$ colocalizes with internalized receptors and $G\beta\gamma$ on early endosomes after GPCR activation*

A prerequisite for GPCRs to increase the concentration of active-state $G\alpha_s$ on endosomes is for $G\alpha_s$ to be present on the relevant endosome membrane. It is generally thought that $G\alpha_s$ dissociates from the plasma membrane after its activation and subsequently samples a variety of intracellular membrane compartments, including endosomes that contain activated GPCRs after regulated endocytosis[19,22,23,25,26]. A second round of GPCR-triggered G protein

activation is then thought to occur on endosomes[4,5,7,9,10]. We sought to verify and further examine this process in living cells. We began by imaging $G\alpha_s$ in living cells by confocal microscopy, using the β2-adrenergic receptor (β2AR) as a model $G_s$-coupled GPCR that is well known to trigger intracellular redistribution of $G\alpha_s$[19,20,22–24]. We labeled $G\alpha_s$ by inserting EGFP into the linker region between its α-helical appendage and conserved Ras-like domain, a strategy shown previously to preserve the signaling function of $G\alpha_s$[24], and we then expressed this labeled construct in HEK293 cells stably expressing Flag-tagged β2AR. Consistent with previous studies from others and us[20,22–24], EGFP-$G\alpha_s$ visibly redistributed intracellularly from the plasma membrane within several minutes after application of the β2AR agonist, isoproterenol (Iso, Fig. 1a). EGFP-$G\alpha_s$ was diffusely distributed in the cytoplasm and concentrated on various endomembranes, including endosomes, as verified by colocalization with mApple-EEA1 (Supplementary Fig. 1a). We previously observed redistribution from the plasma membrane to the cytoplasm, but we were unable to resolve specific internal membrane localization[20]. As these early studies were conducted using epitope-tagged $G\alpha_s$ in fixed cells, we examined fixed cells and found that intracellular membrane localization of EGFP-$G\alpha_s$ was less well-preserved (Supplementary Fig. 1b).

$G\alpha_s$ activation on endosomes would require receptors to be present in the same endosome membrane. Previous studies have reported little or no colocalization between $G\alpha_s$ and internalized β2ARs[22,23], so we tested this in our system by imaging EGFP-$G\alpha_s$ and internalized β2ARs. Confocal microscopy resolved EGFP-$G\alpha_s$ localization on Flag-β2AR-containing endosomes in isoproterenol-treated cells, and we also observed EGFP-$G\alpha_s$ localization on additional compartments not containing internalized receptors (Fig. 1a, arrows indicate examples of EGFP-$G\alpha_s$ / Flag-β2AR colocalization). We quantified colocalization using Pearson correlation analysis, assessing pixel-based correlations between EGFP-$G\alpha_s$ and either the mApple-EEA1 or Flag-β2AR fluorescence signal, respectively, after agonist application. The Pearson correlation coefficient between EGFP-$G\alpha_s$ and mApple-EEA1 increased after receptor activation (Fig. 1b), indicating $G\alpha_s$

redistribution to early endosomes. In contrast, the Pearson correlation coefficient between EGFP-G$\alpha_s$ and Flag-β2AR decreased after agonist application (Fig. 1c), likely representing loss of both Flag-β2AR and EGFP-G$\alpha_s$ from the plasma membrane. However, the Pearson correlation coefficient between EGFP-G$\alpha_s$ and Flag-β2AR plateaued at a level that remained significantly higher than the Pearson correlation between a cytosolic EGFP control and Flag-β2AR (Fig. 1c), consistent with our observations of partial colocalization with receptors on endosomes. Together, these results indicate that activated β2ARs trigger EGFP-G$\alpha_s$ to rapidly redistribute from the plasma membrane to endomembranes, including endosomes that also contain internalized β2ARs.

As G$\alpha_s$ association with Gβγ is a prerequisite for the GPCR coupling reaction that produces active G$\alpha_s$, we asked if Gβγ is present on the same endosomes using a labeled γ-subunit (mApple-G$\gamma_2$) to detect Gβγ. Labeled Gβγ was broadly distributed on the plasma membrane and on multiple internal membranes, including membranes also associated with EGFP-G$\alpha_s$ (Fig. 1d). Whereas endosomal localization of labeled G$\alpha_s$ and β2AR were both markedly increased after β2AR activation, the localization of Gβγ appeared similar both before and after application of isoproterenol (Fig. 1d). These findings support a model in which G$\alpha_s$ and β2AR colocalize on endosomes in an activation-induced manner, and that these endosomes are constitutively associated with Gβγ[27]. Accordingly, all of the protein components necessary for G protein coupling are present on endosomes after agonist-induced activation.

*G$\alpha_s$ returns to the plasma membrane after receptor inactivation*

The ability of cells to respond to a subsequent agonist exposure would presumably require replenishment of G$\alpha_s$ at the plasma membrane, and previous studies have suggested that the intracellular redistribution of G$\alpha_s$ triggered by β2AR activation is reversible after receptor inactivation[19,20]. We sought to verify this by activating Flag-β2AR with Iso in cells coexpressing EGFP-G$\alpha_s$, and then applying the β2AR antagonist Alprenolol (Alp) in excess

to inactivate the receptor. We observed a pronounced reaccumulation of EGFP-G$\alpha_s$ on the plasma membrane after β2AR inactivation (Fig. 2a, Supplementary Fig. 2a), verifying reversibility of the G$\alpha_s$ redistribution process as reported previously by others and us[19,20]. To quantify these effects, we used NanoBit protein complementation to measure the plasma membrane localization of G$\alpha_s$ over time. We inserted LgBit into G$\alpha_s$ at the same position as EGFP (LgBit-G$\alpha_s$) and measured complementation with a plasma membrane-targeted SmBit construct (SmBit-mApple-CAAX), confirming appropriate plasma membrane localization of this construct by confocal microscopy (Supplementary Fig. 2b). In this assay, a net intracellular redistribution of G$\alpha_s$ results in a decrease in the luminescence signal, which is produced by protein complementation (Fig. 2b). Iso-induced activation of Flag-β2AR produced a decrease in luminescence intensity with a similar time course as the redistribution observed by microscopy (Fig. 2c), and this signal recovered to near baseline after reversal of β2AR activation (Fig. 2c). These data verify that net intracellular redistribution of G$\alpha_s$ triggered by β2AR activation is reversible after receptor inactivation, resulting in a net replenishment of the plasma membrane-associated G$\alpha_s$ pool.

*Intracellular redistribution of G$\alpha_s$ does not depend on GPCR endocytosis*

Previous studies differ in whether intracellular redistribution of G$\alpha_s$ triggered by β2ARs requires receptor endocytosis[20,22,23], so we revisited this question using improved tools for monitoring G$\alpha_s$ redistribution. As a first approach, we blocked endocytosis of β2ARs using the dynamin inhibitor Dyngo4a[28]. Iso-induced internalization of Flag-β2AR was strongly suppressed by Dyngo4a treatment; however, intracellular redistribution of EGFP-G$\alpha_s$ was not detectably affected, suggesting that endocytosis of the activating GPCR is not required for GPCR-triggered intracellular redistribution of G$\alpha_s$ (Supplementary Fig. 3a).

As a second approach, we prevented receptor internalization by mutating specific serine residues in the cytoplasmic tail of β2AR to alanine[9,29,30], and we assessed the ability of the

internalization-defective mutant receptor to trigger intracellular redistribution of $G\alpha_s$. HEK293 cells endogenously express β-adrenergic receptors at a low level[31], but this level was not sufficient to produce a detectable Iso-induced redistribution of $G\alpha_s$ in the NanoBit assay (Supplementary Fig. 3b). Thus, we compared the effects of β2AR-3S to WT β2AR when overexpressed at comparable levels (Supplementary Fig. 3c). β2AR-3S triggered intracellular redistribution of $G\alpha_s$ that was indistinguishable from that triggered by WT β2AR (Fig. 2d), and we verified by imaging that β2AR-3S also promoted accumulation of EGFP-$G\alpha_s$ on endomembranes (Supplementary Fig. 3d).

Finally, as a third approach, we examined $G\alpha_s$ redistribution in previously described β-arrestin 1/2 double knockout (*βarr1/2* DKO) HEK293 cells[15]. After verifying a blockade of WT β2AR internalization (Supplementary Fig. 3e), we again observed that Iso treatment triggered robust and reversible intracellular redistribution of $G\alpha_s$ in these cells (Fig. 2e, Supplementary Fig. 3e). Moreover, re-expression of βARR2-mApple in this knockout background fully rescued internalization of Flag-β2AR but did not affect the observed redistribution of $G\alpha_s$ (Fig. 2e, Supplementary Fig. 3e). Together, these results strongly suggest that receptor internalization is not required for the intracellular redistribution of $G\alpha_s$.

*Intracellular redistribution of $G\alpha_s$ is triggered by multiple $G_s$-coupled GPCRs at native levels*

We next asked if the ability to trigger intracellular redistribution of $G\alpha_s$ is shared by other $G_s$-coupled GPCRs. We focused on the adenosine-2B receptor ($A_{2B}R$ or ADORA2B) and vasoactive intestinal peptide-1 receptor (VIPR1 or VPAC1) as representatives of GPCR families A and B, respectively, each of which is natively expressed in HEK293 cells[31]. We found both receptors triggered a pronounced intracellular redistribution of EGFP-$G\alpha_s$ when overexpressed and activated by their cognate agonists (VIP or NECA), similar to that triggered by overexpressed β2AR after activation by Iso (Supplementary Fig. 4).

Because achieving GPCR-triggered redistribution of EGFP-G$\alpha_s$ in these assays required the receptor to be overexpressed, we wondered if G$\alpha_s$ redistribution can also be triggered by native GPCRs or, alternatively, if this redistribution process is an artifact of excessive receptor expression. We reasoned that overexpressing EGFP-G$\alpha_s$ in cells also expressing endogenous, unlabeled G$\alpha_s$ might limit the sensitivity of our assay for detecting redistribution triggered by endogenous receptors, particularly as the level of native receptor expression is far lower than that of G$\alpha_s$[32]. To address this, we expressed EGFP-G$\alpha_s$ at a much lower level in cells lacking native G$\alpha_s$, which we reasoned would likely compete in our assay. We first knocked out endogenous G$\alpha_s$ by CRISPR-Cas9 editing of the *GNAS* gene (G$\alpha_s$ KO cells). Full knockout of G$\alpha_s$ was verified genetically and by immunoblot, as well as functionally by loss of the Iso-induced cytoplasmic cAMP elevation (Supplementary Fig. 5). We then isolated cell populations stably expressing EGFP-G$\alpha_s$ at a low level, within 2-fold of the native level in wild-type cells as assessed by immunoblot, and we verified rescue of the Iso-induced cAMP response in two independent isolates (Supplementary Fig. 6).

This near-native level of EGFP-G$\alpha_s$ expression was detectable by confocal microscopy but quite dim (Supplementary Fig. 6c), so we turned to total internal reflection fluorescence (TIRF) microscopy as a more sensitive and quantitative method for assessing EGFP-G$\alpha_s$ localization. We detected intracellular redistribution of EGFP-G$\alpha_s$ by loss of fluorescence intensity from the evanescent field, in which the bottom plasma membrane surface is selectively illuminated relative to the cell interior. Using this approach, we observed a significant Iso-induced reduction of surface-localized EGFP-G$\alpha_s$ upon stimulation of endogenous β2ARs with Iso, indicating a net intracellular redistribution of EGFP-G$\alpha_s$ from the plasma membrane. The magnitude of this effect was much lower than that observed in the presence of overexpressed β2ARs (Fig. 3 and Supplementary Fig. 7, Supplementary Tables 8 and 9), consistent with a much lower level of endogenous receptor expression. Both VIP and NECA also triggered a significant intracellular redistribution of EGFP-G$\alpha_s$ through their endogenously expressed receptors (Fig. 3 and Supplementary Fig. 7,

Supplementary Tables 8 and 9). Together, these results indicate that a variety of $G_s$-coupled GPCRs share the ability to trigger the intracellular redistribution of $G\alpha_s$, and that they can do so at native or near-native levels of receptor and G protein expression.

*VIPR1 produces active-state $G\alpha_s$ on the plasma membrane and endosomes*

Signaling from endosomes requires $G\alpha_s$ associated with the endosome membrane to be in an active state. The above experiments provided useful information about the net subcellular redistribution of $G\alpha_s$, but they provided no information about its activation state. To address this, we utilized KB1691, a peptide that binds selectively to active-state $G\alpha_s$ and has been used previously as a biosensor for detecting active-state $G\alpha_s$ in cells that overexpress both receptors and $G_s$[33]. We wondered if this peptide can be adapted to resolve the location of active-state $G\alpha_s$ at a native expression level. We tested this by focusing on VIPR1 because this GPCR strongly stimulates sequential $G_s$ signaling phases from the plasma membrane and endosomes[15]. We began by assessing VIP-stimulated recruitment of KB1691 to the plasma membrane, fusing KB1691 to SmBit-mApple (SmBit-mApple-KB1691) and measuring protein complementation with a plasma membrane-targeted LgBit (LgBit-CAAX, Fig. 4a). A clear VIP-induced recruitment signal was detected in cells expressing only native G proteins (Fig. 4b), albeit dependent on VIPR1 being overexpressed. These results verify the utility of KB1691 as a biosensor and indicate that KB1691 is sufficiently sensitive to detect active-state G proteins at native levels in cells that overexpress the activating GPCR.

To test the specificity of sensor recruitment, we used knockout cells lacking $G\alpha_s$, and additionally deleted $G\alpha_{olf}$, a close paralog of $G\alpha_s$ ($G\alpha_{s/olf}$ DKO cells) that we thought might also engage the sensor (Supplementary Fig. 5). The VIP-induced biosensor response was markedly reduced in $G\alpha_{s/olf}$ DKO cells, verifying the ability of the sensor to detect native $G\alpha_s$ activity in our assay (Fig. 4b). However, we were surprised to observe a residual signal remaining in $G\alpha_{s/olf}$ DKO cells that exhibited faster onset and shorter duration (Fig. 4b).

Further, we verified in the same DKO cell background that the VIP-induced cAMP response was abolished, and that it was rescued by EGFP-G$\alpha_s$ re-expression as expected (Supplementary Fig. 5 and 6). Together, these kinetic and genetic data strongly suggest that the sensor detects both active-state G$\alpha_s$ and a distinct, non-$G_s$ component.

As VIPR1 has been observed previously to couple to $G_q$ as well as $G_s$[34], we wondered if this residual signal might represent active-state G$\alpha_q$ and/or G$\alpha_{11}$. Consistent with this possibility, the $G_{q/11}$ inhibitor YM-254890 (YM)[35] eliminated the residual VIP-induced recruitment signal in G$\alpha_{s/olf}$ DKO cells (Fig. 4c). Furthermore, YM selectively blocked the rapid component of biosensor recruitment measured in wild type cells without affecting the slower component (Fig. 4d). Accordingly, in subsequent experiments, we defined the biosensor signal measured in the presence of YM as a specific readout of active-state $G_s$. We interpret the YM-sensitive fraction of the signal simply as a distinct, non-$G_s$ component, which may represent active-state $G_q$ and/or $G_{11}$.

As our primary interest is signaling from endosomes, we next asked if we can detect active-state G proteins at endogenous levels on the endosome membrane. To do so, we modified the assay to measure complementation of SmBit-mApple-KB1691 with an endosome-targeted LgBit construct (endofin-LgBit, Fig. 4e). VIP produced a robust endosomal signal, and with slower kinetics than recruitment on the plasma membrane (Fig. 4f). Interestingly, this endosomal signal was largely unaffected by YM (Fig. 4f), in contrast to the plasma membrane signal, which clearly included a non-$G_s$, YM-sensitive component (Fig. 4d). These results indicate that the biosensor can indeed detect active-state $G_s$ on endosomes, as well as on the plasma membrane, and at native levels. In addition, they suggest that VIPR1 mediates G protein activation in a 'location biased' manner, as defined by the production of two distinguishable activation components ($G_s$ and non-$G_s$) on the plasma membrane but primarily one component ($G_s$) on endosomes.

*Active-state $G\alpha_s$ production on endosomes is endocytosis-dependent*

We next asked if producing active-state $G\alpha_s$ on endosomes requires the presence of activated GPCRs in the endosome membrane. This is expected based on the present understanding that G protein activation on endosomes requires a second GPCR-G protein coupling reaction that occurs locally on the endosome limiting membrane[4,5]. However, we observed that the GPCR-triggered intracellular redistribution of $G\alpha_s$ to endosomes does not require the presence of receptors on endosomes (Fig. 2, Supplementary Fig. 3). Therefore, we wanted to explicitly test whether or not the production of active-state $G\alpha_s$ on endosomes is endocytosis-dependent, taking advantage of the ability of the KB1691-derived biosensor to detect active-state $G\alpha_s$ on endosomes.

To ask this question, we inhibited VIPR1 internalization using dominant negative (K44E) mutant dynamin[15]. Mutant dynamin reduced the amount of active-conformation VIPR1 at endosomes after VIP application, as detected by a previously described active-state GPCR binder (mini-Gs)[15], and it increased the amount of active-state VIPR1 at the plasma membrane (Fig. 5a-c), verifying inhibition of receptor endocytosis. Using the KB1691-derived biosensor, we found that mutant dynamin decreased the active-state $G\alpha_s$ signal specifically on the endosome membrane, and to a comparable degree as the decrease in activated receptors in endosomes (Fig. 5d-f, Supplementary Fig. 8). These observations support the conclusion that the production of active-state $G\alpha_s$ on the endosome membrane requires the presence of activated receptors in endosomes, presumably to mediate local GPCR-G protein coupling.

*Detection of VIPR1-mediated coupling to $G\alpha_s$ on endosomes*

The results described above indicate that the production of active-state $G\alpha_s$ is endocytosis-dependent, consistent with local coupling on endosomes. We next wanted to investigate whether it is possible to directly detect this proposed coupling reaction with native G

proteins. To do so, we adapted the NanoBit assay to detect recruitment of Nb37 rather than KB1691. Nb37 is a nanobody that binds to the N-terminal helical domain of $G\alpha_s$ when destabilized by coupling to receptors or in a nucleotide-free state[36]. This contrasts with KB1691 that binds specifically to the GTP-bound active state[33], and we focused on Nb37 as a proxy measure of the GPCR-G protein coupling reaction[9]. This approach was shown previously to robustly detect coupling on endosomes in cells overexpressıng both VIPR1 and $G_s$[15], and we found it possible to detect coupling in cells expressing native G proteins using the same experimental design provided that VIPR1 was overexpressed (Fig. 6a-c). VIP produced a robust Nb37 recruitment signal both on the plasma membrane and endosomes, and with the expected sequential kinetics (Fig. 6c). These results, which we interpret as an indication of local GPCR-G protein coupling, were similar to those obtained with the KB1691-derived active-state sensor. Together, these results support the hypothesis that the production of active-state $G\alpha_s$ on endosomes is mediated by local receptor coupling at this location.

Because KB1691 detected a non-$G_s$ component of the active-state G protein signal after VIPR1 activation, we wanted to also verify specificity of the coupling signal detected by Nb37. We observed a residual signal that remained in $G\alpha_{s/olf}$ DKO cells, similar to what we observed with KB1691 (Supplementary Fig. 9a). Similar to the non-$G_s$ component detected by the KB1691-derived active-state biosensor, the non-$G_s$ signal detected by Nb37 recruitment was eliminated in the presence of YM (Supplementary Fig. 9b). Accordingly, we used the same strategy to define $G_s$ and non-$G_s$ components. Using this approach, we again resolved both $G_s$ and non-$G_s$ components of VIPR1-mediated coupling on the plasma membrane, but primarily a $G_s$ component on endosomes (Fig. 6c). These results provide independent support for the hypothesis that endosomal $G_s$ activation is mediated by a local coupling reaction on the endosome limiting membrane, and they verify the existence of distinct $G_s$ and non-$G_s$ components of G protein activation by VIPR1 on the plasma membrane.

*The location bias of G protein activation on endosomes is GPCR-specific*

Our results with VIPR1 support the model that local GPCR-G protein coupling is needed to produce active-state $G\alpha_s$ on endosomes. As an additional approach to test this idea, we took advantage of the fact that the human $A_{2B}R$ internalizes weakly after agonist-induced activation relative to VIPR1[31]. If local coupling to activated receptors is required for endosomal G protein activation to occur, we predicted that the $A_{2B}R$ would produce a relatively weak $G_s$ coupling signal on endosomes. This was indeed the case. $A_{2B}R$ activation by NECA clearly produced both $G_s$ and non-$G_s$ components of Nb37 recruitment at the plasma membrane, but little or no signal representing $G_s$ coupling was detected on endosomes (Fig. 6d, Supplementary Fig. 9cd). These results provide additional support for the model that endosomal activation of $G\alpha_s$ requires local receptor-$G_s$ coupling.

While $A_{2B}R$ activation produced little or no $G_s$ coupling signal on endosomes, it did produce a detectable non-$G_s$ component (Fig. 6d). This further supports the concept of location bias in G protein coupling on endosomes, relative to the plasma membrane. Remarkably, $A_{2B}R$ produced largely the non-$G_s$ coupling signal on endosomes, in contrast to VIPR1, which produced largely the $G_s$ component, but each GPCR produced both components on the plasma membrane. These results further suggest that distinct GPCR family members are able to differentially bias endosomal G protein activation in a receptor-specific manner (Fig. 7).

## Discussion

Many GPCRs are now known to exist in an activated conformation on both endomembranes and the plasma membrane[5], and there is substantial evidence that they can produce distinct and additional signaling effects from endomembranes[8,31,37–46]. Such signaling requires GPCRs to increase G protein activity on the appropriate endomembrane compartment, but

how this is achieved remains unclear. We investigated this question by focusing on how $G_s$-coupled receptors control G protein abundance and activity on endosomes.

The ability of $G_s$ to redistribute between membranes was proposed more than 40 years ago based on in vitro biochemical reconstitution[47]. Multiple groups have since demonstrated redistribution of $G\alpha_s$ in intact cells and provided insight into its mechanistic basis[19–24]. Here, we began by verifying the present view that 1) $G_s$-coupled GPCRs trigger the rapid redistribution of $G\alpha_s$ from the plasma membrane to sample various intracellular membranes, including endosomes, 2) this process is reversible, and 3) it does not require the triggering GPCR to internalize[19,22]. We then build on this understanding by showing that a number of $G_s$-coupled GPCRs can trigger this intracellular redistribution process at native receptor expression levels. We next carried out a series of experiments to investigate location-specific regulation of endosomal $G\alpha_s$ activity using conformational biosensors, and we demonstrate that this approach is capable of detecting and localizing active-state $G\alpha_s$ at native G protein levels.

Our results support a simple model in which the abundance and activity of $G\alpha_s$ on endosomes are separately controlled by distinct GPCR-G protein coupling reactions occurring at different subcellular locations–with coupling on the plasma membrane increasing endosomal $G\alpha_s$ abundance and local coupling on endosomes increasing endosomal $G\alpha_s$ activity (Fig. 7a). We detect a small amount of $G\alpha_s$ on endosomes in cells prior to agonist exposure, as noted previously by others[19,27]. Thus, it remains to be determined if the first coupling reaction, which increases $G\alpha_s$ abundance on endosomes, is necessary for signaling from endosomes, or if the basal level of endosomal $G_s$ abundance is sufficient. We note that previous studies have come to different conclusions on this question, albeit based on studies of different G protein classes[18,19].

To our knowledge, the present results are the first to detect and localize active-state $G\alpha_s$ in intact cells expressing only native G proteins. In evaluating the specificity of the biosensors used to achieve this, we were surprised to observe that both biosensors detect a distinct non-$G_s$ component, defined by its different kinetics and stimulation in $G\alpha_{s/olf}$ DKO cells. We currently speculate that this component represents activation of $G_q$ and/or $G_{11}$ because it is eliminated by YM, but further study will be necessary to more fully define this component and investigate its potential functional significance. Whereas both VIPR1 and $A_{2B}R$ produced both components at the plasma membrane, they selectively produced one component or the other on endosomes in a receptor-specific manner (Fig. 7b). These results support the existence of 'location bias' in GPCR-G protein coupling selectivity on endomembranes, consistent with previous evidence for such bias both through assays of functional signaling[7,48] and recruitment of different biosensors of GPCR activation[49–51]. Further, they suggest that this location bias is GPCR-specific.

It is also remarkable that $A_{2B}R$ produces a detectable non-$G_s$ coupling signal on endosomes, despite this GPCR internalizing only weakly when compared to VIPR1[31]. This observation is consistent with a previous study indicating that $G_{q/11}$ activation on endosomes can occur even when the concentration of activated receptors in endosomes is reduced to a low level by endocytic inhibition[18]. We also note emerging evidence for the existence of a second cellular mechanism of $G_{i/o}$ activation on endosomes that does not depend on the activating GPCRs being present in endosomes[52].

In closing, the present results add to the currently expanding mechanistic framework of spatiotemporal GPCR signaling through heterotrimeric G protein. They also raise new questions that may help to guide further elucidation of this process and enable its future therapeutic manipulation.

## Methods

*Cell culture and transfections*

HEK293 cells were purchased from ATCC (CRL-1573) and cultured in DMEM (Gibco 11965-092) and 10 % FBS (R&D Systems, S12495) at 37 °C and 5 % $CO_2$ in a humid environment. All cell lines used in this study were generated from HEK293 cells, with the exception of HEK293A *GNAS/GNAL* double knockout[53] cells used in Supplementary Figure 5. Polyclonal cells stably expressing Flag-β2AR[31] were cultured in 500 µg/mL geneticin (Gibco 10131027). All cell lines were routinely screened for mycoplasma contamination (MycoAlert, Lonza LT07-318). Cells were transfected using Lipofectamine 2000 (Thermo Fisher 11668019) according to the manufacturer's protocol. For experiments in Figure 5 and Supplementary Figure 8, cells were transfected with appropriate receptor and nanobit pairs and transduced after four hours with either mCherry or mCherry-Dynamin-1 K44E BacMam diluted in culture media.

*DNA constructs and molecular cloning*

All DNA constructs used in this study are listed in Supplementary Table 1. Novel constructs were constructed by standard InFusion (Takara Bio) or KLD (NEB) cloning techniques, following the manufacturers' protocols, and sequences were confirmed by Sanger sequencing. mCherry and mCherry-Dynamin-1 K44E BacMam produced from pCMV-Dest (Thermo Fisher A24223) used in Figure 5 and Supplementary Figure 8 were produced according to the manufacturer's protocol.

*Generation of CRISPR KO cell lines*

Single guide RNAs (sgRNAs) were designed with the Synthego CRISPR design tool (Supplementary Table 2). To generate ribonucleoproteins (RNPs), 3 µL of 53.3 µM sgRNA (Synthego) were mixed with 2 µL of 40 µM Cas9 (UC Berkeley Macrolab) and incubated at room temperature for 10 minutes. Cells ($2.0 \times 10^5$) were prepared for electroporation with RNPs with the SF Cell Line 4D Nucleofector kit (Lonza) following the manufacturer's protocol and electroporated in a 4D Nucleofector (Lonza) using program CM-130. After electroporation, monoclonal cell lines were established using standard techniques and genetic modifications were verified using either Sanger sequencing or next-generation sequencing (Amplicon-EZ, Azenta Life Sciences, see Supplementary Table 3 for NGS primers). For novel $G\alpha_{s/olf}$ DKO cells, modifications were done sequentially.

*Generation of EGFP-$G\alpha_s$ KO cell lines*

$G\alpha_s$ KO1 and KO2 cells were transfected with EGFP-$G\alpha_s$ and selected with 500 µg/mL geneticin. After selection, cells expressing EGFP-$G\alpha_s$ were sorted into a polyclonal population using a FACSAria Fusion Flow Cytometer (BD Biosciences, KO1) or FACSAria III flow cytometer (BD Biosciences, KO2). Cells were cultured under continued selection.

*Live cell confocal microscopy*

Confocal imaging was performed using a fully automated Nikon Ti inverted microscope equipped with a CSU-22 spinning disk (Yokogawa), piezo stage (Mad City Labs), 4-line Coherent OBIS laser launch (100 mW at 405, 488, 561, and 640 nM), a quad dichroic 405/491/561/640 (Yokogawa), and corresponding emission filters ET460/50m, ET525/50m, ET610/60m, ET700/75m in a filter wheel controlled by a Lambda 10-3B (Sutter) for channels DAPI/GFP/RFP/Cy5, respectively. Images were captured using an Apo TIRF 100x/1.49 oil

objective lens (Nikon) and a Photometrics Evolve Delta EMCCD Camera (154 nm/pixel) controlled with Nikon NIS Elements HC v.5.21.03 software.

For live imaging, cells grown in either 6-well plates or 6 cm dishes were transfected 48 hours before imaging and plated into 35 mm glass bottom microscopy dishes (Cellvis D35-20-1.5-N) coated with 0.001 % (w/v) poly-L-lysine (Millipore Sigma P8920) 24 hours after transfection. Receptors were surface labelled with either monoclonal anti-Flag M1 antibody (Millipore Sigma F3040) labelled with Alexa Fluor 647 (Thermo Fisher A20186) or 200 nM $JF_{635}$i-HTL[54] for 10 minutes at 37 °C and 5 % $CO_2$. After labelling, cells were washed three times and imaged in imaging media (DMEM (no phenol red, Gibco 31053-028) supplemented with 30 mM HEPES pH 7.4) in a temperature- and humidity-controlled chamber at 37 °C (OkoLab). Time-lapse images in Figure 1, Supplementary Figure 1, Supplementary Figure 3, and Supplementary Figure 4 were acquired by imaging cells at 20 second intervals for 30 minutes, and agonist (specified in figure legends) was added after 5 minutes. In Supplementary Figure 3a, cells were treated with either Dyngo4a (30 μM, Abcam ab120689) or DMSO (0.1 %) for 25 minutes prior to imaging, Alexa Fluor 647 coupled anti-Flag M1 antibody was added for the last 10 minutes of pretreatment, and cells were washed and imaged in imaging media containing either Dyngo4a or DMSO. For time lapse images in Figure 2 and Supplementary Figure 2, cells were imaged at 20 second intervals for 60 minutes with 100 nM Iso added at 5 minutes and 10 μM Alp added at 15 minutes.

Images were processed for presentation in Fiji v2.14[55]. Pearson correlation analysis was performed using Cell Profiler v4.2.6[56]; briefly, cells were segmented based on the green channel for each frame and Pearson correlation was calculated between channels at each time point.

*Fixed imaging*

Cells were transfected in 6 well plates 48 hours before fixation. After 24 hours, cells were split onto coverslips coated with 0.001 % poly-L-lysine (Millipore Sigma P8920) in 12 well plates and grown for an additional 24 hours. Cells were then surface labelled with monoclonal anti-Flag M1 antibody (Millipore Sigma F3040) labelled with Alexa Fluor 647 (Thermo Fisher A20186) for 10 minutes at 37 °C and 5 % $CO_2$. After labelling, cells were washed two times with full media (DMEM + 10 % FBS) and treated with either vehicle or Iso (1 μM) for an additional 15 minutes at 37 °C and 5 % $CO_2$. Cells were then placed on ice, washed 1x with DPBS, and fixed at room temperature for 10 minutes in 3.7 % formaldehyde in modified BRB80 (80 mM PIPES pH 6.8, 1 mM $MgCl_2$, 1 mM $CaCl_2$). After fixation, cells were washed 3 times with DPBS, incubated in TBS for 20 minutes, and washed an additional 3 times with DPBS. Dapi (1:5000) was included in the final wash. Cells were then mounted in ProLong Gold Antifade mounting medium and left to dry overnight in the dark. Slides were imaged using the confocal microscope described above using a Plan Apo VC 60x/1.4 oil objective lens. Images were processed for presentation using Fiji v2.14[55].

*TIRF microscopy*

For live cell TIRF microscopy, cells were imaged using the same methods as for live cell confocal microscopy. Images were acquired on a fully automated inverted Nikon Ti-E microscope controlled by Nikon NIS-Elements software (5.20.00 build 1423), a Nikon motorized stage equipped with a TIRF module with STORM lens (Nikon), Agilent MLC400 (405nm, 488nm, 561nm, 647nm) light source with NIDAQ interface (v18.00), and corresponding emission filters ET455/50m, ET525/50m, ET600/60m, ET705/72m in a filter wheel controlled by a Lambda 10-3B (Sutter) for channels DAPI/GFP/RFP/Cy5, respectively. Images were captured using an Apo TIRF 100x/1.49 objective (Nikon) with an Andor DU897 EMCCD camera and an OkoLab temperature controlled live stage insert. Time lapse images

were acquired at 10 second intervals for 25 minutes at 37 °C with agonist added at 5 minutes.

Images were analyzed and processed for presentation using Fiji v2.14[55]. To quantify relative changes in surface fluorescence ($F/F_0$), cells were manually segmented by drawing a region of interest (ROI) around the cell surface. The mean, background subtracted, fluorescence intensity (F) was measured at each time point and normalized to the average mean fluorescence intensity before agonist treatment ($F_0$). To calculate vehicle subtracted $F/F_0$ values, the $F/F_0$ of vehicle control replicates were averaged at each time point and subtracted from the $F/F_0$ values at each time point for individual movies. For presentation in Figure 3 and Supplementary Figure 7, images were scaled to the pre-agonist time point and pseudo-colored using the viridis colormap in Fiji to visualize relative changes in fluorescence.

*NanoBit luciferase complementation assays*

Cells were grown in 6-well plates or 6 cm dishes and transfected with both receptor constructs (Flag-β2AR, Halo-VIPR1, or Halo-$A_{2B}$R) and the appropriate LgBit- and SmBit-tagged constructs (in Nb37 assays shown in Figure 6 and Supplementary Figure 9, the SmBit(101) tag was used, while the SmBit(114) tag was used in all other assays[57]). After 24 hours, cells were washed, lifted, spun at 500 x g for 3 minutes and resuspended in assay buffer (20 mM HEPES pH 7.4, 135 mM NaCl, 5 mM KCL, 0.4 mM $MgCl_2$, 1.8 mM $CaCl_2$) with 5 μM coelenterazine-H (Research Product International C61500). Cells were plated (100 μL) into untreated white 96-well plates (Corning 3912) and incubated at 37 °C and 5 % $CO_2$ for either 10 minutes or 30 minutes (for cells pretreated with DMSO (0.1 %) or YM-254890 (1 μM, Cayman Chemical 29735 or Tocris 7352), as indicated in figure legends) before reading. Luminescence was measured on either a Synergy H4 (BioTek, for data in Figure 2 and Supplementary Figure 3) or Spark (Tecan, for all other data) plate reader. For

assays in Figure 2, luminescence was read every 1 minute for a 5-minute baseline, after which either vehicle or Iso (100 nM) was added and luminescence read for 10 minutes, followed by vehicle or Alp (10 μM) addition and additional luminescence reading for 30 minutes. For assays in Supplementary Figure 3, luminescence was read every 1 minute for a 5-minute baseline, after which either vehicle or Iso (1 μM) was added and luminescence read for an additional 30 minutes. For all other assays, luminescence was read every 30 seconds for a 5-minute baseline, after which vehicle or agonist (noted in figure legends) was added and luminescence measured for an additional 30 minutes. For cells pretreated with DMSO or YM-254890, cells were kept in continual treatment for the duration of the assay.

To analyze data, the change in normalized luminescence was calculated by normalizing each well to its average baseline luminescence. Then, the average change of luminescence of vehicle-treated wells was subtracted from the average change in luminescence of agonist-treated cells. Data are represented as the vehicle subtracted change in luminescence of agonist-treated cells ($\Delta Lum = Lum_{agonist} - Lum_{vehicle}$).

*cADDis cAMP assays*

Intracellular cAMP levels were measured using either Green Up cADDis cAMP biosensor (Montana Molecular U02006, Supplementary Figure 5) or Red Up cADDis cAMP biosensor (Montana Molecular U0200R, Supplementary Figure 6) following the manufacturer's protocol. Briefly, 50,000 cells were plated into TC-treated black 96-well plates (Corning 3340) coated with 0.001 % (w/v) poly-L-lysine (Millipore Sigma P8920) and transduced with cADDis BacMam. After 24 hours, cells were washed with assay buffer (20 mM HEPES pH 7.4, 135 mM NaCl, 5 mM KCL, 0.4 mM $MgCl_2$, 1.8 mM $CaCl_2$) twice and incubated at 37 °C in a temperature controlled plate reader (Tecan Spark for Green cADDis assays or BioTek Synergy H4 for Red cADDis assays). Baseline fluorescence was read with an excitation wavelength at 500 nm (Green cADDis) or 558 nm (Red cADDis) and emission wavelength at

530 nm (Green cADDis) or 603 nm (Red cADDis) for 5 minutes every 30 seconds, after which agonist (noted in figure legends) was added and fluorescence read for an additional 30 minutes. To calculate the change in intracellular cAMP ($\Delta F/F_0$), the average baseline fluorescence for each well was calculated ($F_0$) and the change in fluorescence for each well ($\Delta F = F - F_0$) was normalized to $F_0$.

*Immunoblotting*

Cells were lysed in RIPA buffer (50 mM Tris pH 7.4, 150 mM NaCl, 1 % Triton X-100, 0.5 % sodium deoxycholate, 0.1 % SDS) supplemented with Roche cOmplete EDTA-free protease inhibitor tablets (Roche 04693159001) and lysate was boiled at 95 °C for 5 minutes in NuPage LDS Sample Buffer (Thermo Fisher, NP0007) and 20 mM DTT. For Flag-β2AR blots in Supplementary Figure 3, lysate was incubated with LDS Sample Buffer and 20 mM DTT for 1 hour at room temperature instead of boiled at 95 °C. SDS-PAGE and western blots were performed using standard techniques with a polyclonal rabbit anti-$G\alpha_{s/olf}$ antibody (LS-Bio LS-B4790, 1:1000, blocked in Tris-buffered saline, 5 % milk, 0.1 % Tween-20), a monoclonal rabbit anti-GAPDH antibody (D16H11, Cell Signaling Technology 5174S, 1:1000, blocked in LICOR Intercept (TBS) blocking buffer (Licor 927-60001), a monoclonal rabbit βARR1/2 antibody (D24H9, Cell Signaling Technology 4674, 1:1000, blocked in LICOR Intercept (TBS) blocking buffer), or a monoclonal mouse anti-Flag M1 antibody (Millipore Sigma F3040, 1:1000, blocked in LICOR Intercept (TBS) blocking buffer), followed by IRDye 800- or 680-linked anti-mouse or anti-rabbit IgG secondary antibodies (LI-COR Biosciences). Blots were imaged using an Odyssey Imager (v.2.0.3, LI-COR Biosciences) and quantified using Fiji (v2.14).

*Statistical analysis and reproducibility*

Microscopy quantification data are presented as mean ± S.E.M. of individual dishes from at least 3 independent experiments (with the exception of Figure 3b, which are mean ± S.E.M. of individual dishes from at least 2 independent experiments), while cAMP and NanoBit data are presented as mean ± S.D. from at least 3 independent experiments. Each biological replicate in cAMP and NanoBit assays represents the average of at least 2 technical replicates. All images are representative of at least three biologically independent experiments, with the following exceptions: images in Figure 3a, which are representative of at least two independent experiments, and images in Supplementary Figure 2b, Supplementary Figure 4, and Supplementary Figure 6, which are representative of two independent experiments. Statistical tests and area under the curve calculations were performed using GraphPad Prism (v.9 and v.10).

**Data availability**

Data and materials are available upon request.

**References**


1. Pierce, K. L., Premont, R. T. & Lefkowitz, R. J. Seven-transmembrane receptors. *Nat. Rev. Mol. Cell Biol.* **3**, 639–650 (2002).
2. Hilger, D., Masureel, M. & Kobilka, B. K. Structure and dynamics of GPCR signaling complexes. *Nat. Struct. Mol. Biol.* **25**, 4–12 (2018).
3. Lorente, J. S. *et al.* GPCR drug discovery: new agents, targets and indications. *Nat. Rev. Drug Discov.* (2025) doi:10.1038/s41573-025-01139-y.
4. Ripoll, L., von Zastrow, M. & Blythe, E. E. Intersection of GPCR trafficking and cAMP signaling at endomembranes. *J. Cell Biol.* **224**, (2025).
5. Calebiro, D., Miljus, T. & O'Brien, S. Endomembrane GPCR signaling: 15 years on, the

quest continues. *Trends Biochem. Sci.* (2024) doi:10.1016/j.tibs.2024.10.006.

6. Calebiro, D. *et al.* Persistent cAMP-signals triggered by internalized G-protein-coupled receptors. *PLoS Biol.* **7**, (2009).
7. Ferrandon, S. *et al.* Sustained cyclic AMP production by parathyroid hormone receptor endocytosis. *Nat. Chem. Biol.* **5**, 734–742 (2009).
8. Feinstein, T. N. *et al.* Noncanonical control of vasopressin receptor type 2 signaling by retromer and arrestin. *J. Biol. Chem.* **288**, 27849–27860 (2013).
9. Irannejad, R. *et al.* Conformational biosensors reveal GPCR signalling from endosomes. *Nature* **495**, 534–538 (2013).
10. Thomsen, A. R. B. *et al.* GPCR-G Protein-β-Arrestin Super-Complex Mediates Sustained G Protein Signaling. *Cell* **166**, 907–919 (2016).
11. Irannejad, R. *et al.* Functional selectivity of GPCR-directed drug action through location bias. *Nat. Chem. Biol.* **13**, 799–806 (2017).
12. Godbole, A., Lyga, S., Lohse, M. J. & Calebiro, D. Internalized TSH receptors en route to the TGN induce local Gs-protein signaling and gene transcription. *Nat. Commun.* **8**, (2017).
13. Puri, N. M., Romano, G. R., Lin, T. Y., Mai, Q. N. & Irannejad, R. The Organic Cation Transporter 2 Regulates Dopamine D1 Receptor Signaling at the Golgi Apparatus. *eLife* **11**, 1–24 (2022).
14. Daly, C. *et al.* β-Arrestin-dependent and -independent endosomal G protein activation by the vasopressin type 2 receptor. *eLife* **12**, (2023).
15. Blythe, E. E. & von Zastrow, M. β-Arrestin-independent endosomal cAMP signaling by a polypeptide hormone GPCR. *Nat. Chem. Biol.* **20**, 323–332 (2024).
16. Kotowski, S. J., Hopf, F. W., Seif, T., Bonci, A. & von Zastrow, M. Endocytosis Promotes Rapid Dopaminergic Signaling. *Neuron* **71**, 278–290 (2011).
17. Stoeber, M. *et al.* A Genetically Encoded Biosensor Reveals Location Bias of Opioid Drug Action. *Neuron* **98**, 963-976.e5 (2018).
18. Wright, S. C. *et al.* BRET-based effector membrane translocation assay monitors GPCR-

promoted and endocytosis-mediated Gqactivation at early endosomes. *Proc. Natl. Acad. Sci. U. S. A.* **118**, 1–10 (2021).

19. Martin, B. R. & Lambert, N. A. Activated G protein Gαs samples multiple endomembrane compartments. *J. Biol. Chem.* **291**, 20295–20302 (2016).
20. Wedegaertner, P. B., Bourne, H. R. & Von Zastrow, M. Activation-induced subcellular redistribution of G(sα). *Mol. Biol. Cell* **7**, 1225–1233 (1996).
21. Thiyagarajan, M. M. *et al.* Activation-induced subcellular redistribution of Gαs is dependent upon its unique N-terminus. *Biochemistry* **41**, 9470–9484 (2002).
22. Hynes, T. R., Mervine, S. M., Yost, E. A., Sabo, J. L. & Berlot, C. H. Live cell imaging of Gs and the β2-adrenergic receptor demonstrates that both αs and β 1γ7 internalize upon stimulation and exhibit similar trafficking patterns that differ from that of the β2-adrenergic receptor. *J. Biol. Chem.* **279**, 44101–44112 (2004).
23. Allen, J. A., Yu, J. Z., Donati, R. J. & Rasenick, M. M. β-adrenergic receptor stimulation promotes Gαs internalization through lipid rafts: A study in living cells. *Mol. Pharmacol.* **67**, 1493–1504 (2005).
24. Yu, J. Z. & Rasenick, M. M. Real-time visualization of a fluorescent Gαs: Dissociation of the activated G protein from plasma membrane. *Mol. Pharmacol.* **61**, 352–359 (2002).
25. Ransnas, L. A., Svoboda, P., Jasper, R. & Insel, P. A. Stimulation of β-adrenergic receptors of S49 lymphoma cells redistributes the α subunit of the stimulatory G protein between cytosol and membranes. *Proc. Natl. Acad. Sci. U. S. A.* **86**, 7900–7903 (1989).
26. Levis, M. J. & Bourne, H. R. Activation of the alpha subunit of Gs in intact cells alters its abundance, rate of degradation, and membrane avidity. *J. Cell Biol.* **119**, 1297–1307 (1992).
27. Jang, W., Senarath, K., Feinberg, G., Lu, S. & Lambert, N. A. Visualization of endogenous G proteins on endosomes and other organelles. *eLife* (2024) doi:10.7554/eLife.97033.2.
28. Howes, M. T. *et al.* Clathrin-independent carriers form a high capacity endocytic sorting system at the leading edge of migrating cells. *J. Cell Biol.* **190**, 675–691 (2010).

29. Hausdorff, W. P. *et al.* A small region of the beta-adrenergic receptor is selectively involved in its rapid regulation. *Proc. Natl. Acad. Sci.* **88**, 2979–2983 (1991).
30. Trester-Zedlitz, M., Burlingame, A., Kobilka, B. & von Zastrow, M. Mass Spectrometric Analysis of Agonist Effects on Posttranslational Modifications of the β-2 Adrenoceptor in Mammalian Cells. *Biochemistry* **44**, 6133–6143 (2005).
31. Blythe, E. E., Fagan, R. R. & von Zastrow, M. Endocytosis sculpts distinct cAMP signal transduction by endogenously coexpressed GPCRs. (2025) doi:10.1101/2025.02.24.639927.
32. Cho, N. H. *et al.* OpenCell: Endogenous tagging for the cartography of human cellular organization. *Science* **375**, (2022).
33. Janicot, R. *et al.* Direct interrogation of context-dependent GPCR activity with a universal biosensor platform. *Cell* **187**, 1527-1546.e25 (2024).
34. Sreedharan, S. P., Patel, D. R., Xia, M. H., Ichikawa, S. & Goetzl, E. J. Human Vasoactive Intestinal Peptide1 Receptors Expressed by Stable Transfectants Couple to 2 Distinct Signaling Pathways. *Biochem. Biophys. Res. Commun.* **203**, 141–148 (1994).
35. Nishimura, A. *et al.* Structural basis for the specific inhibition of heterotrimeric G q protein by a small molecule. doi:10.1073/pnas.1003553107/-/DCSupplemental.
36. Westfield, G. H. *et al.* Structural flexibility of the Gαs α-helical domain in the β 2-adrenoceptor Gs complex. *Proc. Natl. Acad. Sci. U. S. A.* **108**, 16086–16091 (2011).
37. Tsvetanova, N. G. & von Zastrow, M. Spatial encoding of cyclic AMP signaling specificity by GPCR endocytosis. *Nat. Chem. Biol.* **10**, 1061–1065 (2014).
38. Tsvetanova, N. G. *et al.* Endosomal cAMP production broadly impacts the cellularphosphoproteome. *J. Biol. Chem.* **297**, 100907 (2021).
39. Klauer, M. J., Willette, B. K. A. & Tsvetanova, N. G. Functional diversification of cell signaling by GPCR localization. *J. Biol. Chem.* **300**, (2024).
40. Jensen, D. D. *et al.* Neurokinin 1 receptor signaling in endosomes mediates sustained nociception and is a viable therapeutic target for prolonged pain relief. *Sci. Transl. Med.* **9**, (2017).

41. Yarwood, R. E. *et al.* Endosomal signaling of the receptor for calcitonin gene-related peptide mediates pain transmission. *Proc. Natl. Acad. Sci. U. S. A.* **114**, 12309–12314 (2017).
42. Lyga, S. *et al.* Persistent cAMP signaling by internalized LH receptors in ovarian follicles. *Endocrinology* **157**, 1613–1621 (2016).
43. Kuna, R. S. *et al.* Glucagon-like peptide-1 receptor-mediated endosomal cAMP generation promotes glucose-stimulated insulin secretion in pancreatic-cells. *Am J Physiol Endocrinol Metab* **305**, 161–170 (2013).
44. Girada, S. B. *et al.* Gαs regulates Glucagon-Like Peptide 1 Receptor-mediated cyclic AMP generation at Rab5 endosomal compartment. *Mol. Metab.* **6**, 1173–1185 (2017).
45. White, A. D. *et al.* Spatial bias in cAMP generation determines biological responses to PTH type 1 receptor activation. *Sci. Signal.* **14**, (2021).
46. Lin, T.-Y. *et al.* Cardiac contraction and relaxation are regulated by distinct subcellular cAMP pools. *Nat. Chem. Biol.* (2023) doi:10.1038/s41589-023-01381-8.
47. Rodbell, M. Programmable messengers: a new theory of hormone action. *Trends Biochem. Sci.* 461–464 (1985).
48. Gorvin, C. M. *et al.* AP2σ Mutations Impair Calcium-Sensing Receptor Trafficking and Signaling, and Show an Endosomal Pathway to Spatially Direct G-Protein Selectivity. *Cell Rep.* **22**, 1054–1066 (2018).
49. Hernandez, E. H., Manglik, A. & Irannejad, R. Anionic phospholipids determine G protein coupling selectivity at distinct subcellular membrane compartments. *bioRxiv* (2023) doi:10.1101/2023.08.31.555797.
50. Crilly, S. E., Ko, W., Weinberg, Z. Y. & Puthenveedu, M. A. Conformational specificity of opioid receptors is determined by subcellular location irrespective of agonist. *eLife* **10**, (2021).
51. Radoux-Mergault, A., Oberhauser, L., Aureli, S., Luigi Gervasio, F. & Stoeber, M. *Subcellular Location Defines GPCR Signal Transduction*. https://www.science.org (2023).

52. Fisher, N. M. & Von Zastrow, M. Opioid receptors reveal a discrete cellular mechanism of endosomal G protein activation. *Proc. Natl. Acad. Sci.* **122**, e2420623122 (2025).
53. Stallaert, W. *et al.* Purinergic receptor transactivation by the β2-adrenergic receptor increases intracellular Ca2+ in nonexcitable cells. *Mol. Pharmacol.* **91**, 533–544 (2017).
54. Jonker, C. T. H. *et al.* Accurate measurement of fast endocytic recycling kinetics in real time. *J. Cell Sci.* **133**, (2020).
55. Schindelin, J. *et al.* Fiji: An open-source platform for biological-image analysis. *Nat. Methods* **9**, 676–682 (2012).
56. Stirling, D. R. *et al.* CellProfiler 4: improvements in speed, utility and usability. *BMC Bioinformatics* **22**, (2021).
57. Dixon, A. S. *et al.* NanoLuc Complementation Reporter Optimized for Accurate Measurement of Protein Interactions in Cells. *ACS Chem. Biol.* **11**, 400–408 (2016).
58. Dai, S. A. *et al.* State-selective modulation of heterotrimeric Gαs signaling with macrocyclic peptides. *Cell* **185**, 3950-3965.e25 (2022).
59. Cao, T. T., Deacon, H. W., Reczek, D., Bretscher, A. & von Zastrow, M. A kinase-regulated PDZ-domain interaction controls endocytic sorting of the β2-adrenergic receptor. *Nature* **401**, 286–290 (1999).
60. Shaner, N. C. *et al.* Improving the photostability of bright monomeric orange and red fluorescent proteins. *Nat. Methods* **5**, 545–551 (2008).
61. Xu, Z. *et al.* Structural basis of sphingosine-1-phosphate receptor 1 activation and biased agonism. *Nat. Chem. Biol.* **18**, 281–288 (2022).
62. Eichel, K., Jullié, D. & Von Zastrow, M. β-Arrestin drives MAP kinase signalling from clathrin-coated structures after GPCR dissociation. *Nat. Cell Biol.* **18**, 303–310 (2016).

**Acknowledgements**

We thank Nicole Fisher for sharing plasmids; Asuke Inoue and Luke Lavis for sharing reagents and advice; Aashish Manglik for sharing equipment; and Natalia Jura, Roshanak Irannejad, Barbara Panning, Rita Fagan, Nicole Fisher, and the rest of the von Zastrow lab for helpful discussion and feedback on the manuscript. Imaging data for this study were acquired at the UCSF Center for Advanced Light Microscopy (Nico Stuurman, Kari Herrington, Micaela Lasser, DeLaine Larsen, and SoYeon Kim). The UCSF Helen Diller Family Comprehensive Cancer Center Laboratory for Cell Analysis (Sarah Elmes, supported by the NIH under award P30CA082103) assisted with cell line generation. This work was supported by the NIH under awards R01DA010711 and R01DA012864 (to M.v.Z.). B.W. was supported by T32GM007810.

**Author contributions**

B.W. and M.v.Z. conceptualized the study. B.W., E.E.B., and M.v.Z. designed experiments. B.W. and E.E.B. performed experiments and analyzed data. B.W. and M.v.Z. wrote the manuscript with input from all authors.

**Competing interests**

The authors declare no competing interests.

Correspondence and request for materials should be made to Mark von Zastrow.

## Figures

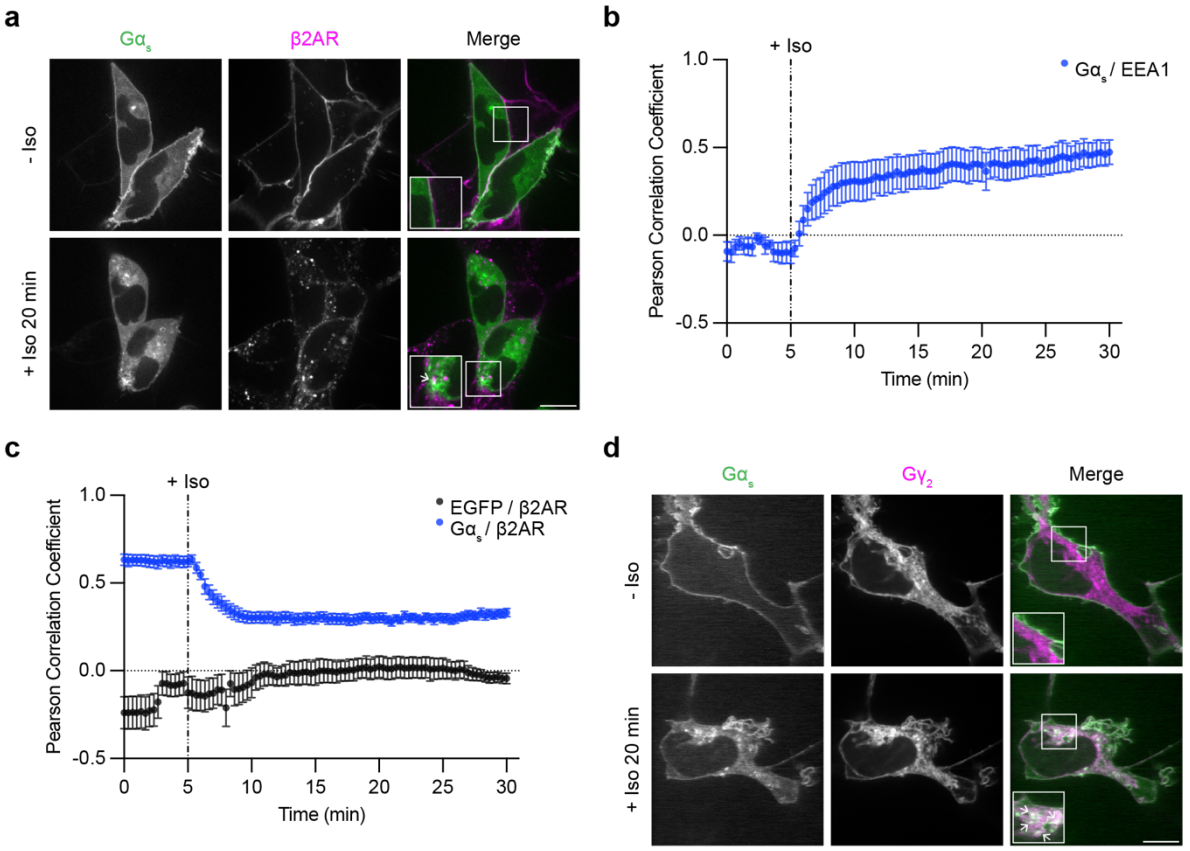


**Figure 1: Gα$_s$ colocalizes with internalized β2ARs and Gβγ on endosomes after receptor activation. a)** Representative confocal images of live HEK293 cells stably expressing Flag-β2AR and transiently expressing EGFP-Gα$_s$ before and after 20 minutes of Iso (1 μM) treatment. **b)** Pearson correlation coefficient between Gα$_s$ and mApple-EEA1 channels over time. Images are shown in Supplementary Fig. 1a. **c)** Pearson correlation coefficient between Gα$_s$ and either the Flag-β2AR or EGFP channels over time. Significance determined by repeated measures 2-way ANOVA with Sidak's multiple comparisons test (see Supplementary Table 4 for p values). **d)** Representative confocal images of live HEK293 cells stably expressing Flag-β2AR and transiently expressing EGFP-Gα$_s$ and mApple-Gγ$_2$ before and after 20 minutes of Iso (1 μM) treatment. Images are representative of at least 3 independent experiments. Prior to imaging, cells were treated for 10 minutes with an anti-Flag antibody coupled to Alexa Fluor 647 to label surface Flag-β2AR. In panel a, cells were co-transfected with myc-Gβ$_1$ and untagged Gγ$_2$. In panel d, cells were cotransfected with untagged Gβ$_1$. Scale bars = 10 μm. Insets in panels a and d are 1.5x zoom of indicated regions and arrows indicate examples of colocalization. For Pearson correlation analysis, data are represented as mean ± S.E.M. of individual dishes (n = 6-16) from at least 3 independent experiments. Iso (1 μM) was added after 5 minutes of imaging, depicted by the dashed line.

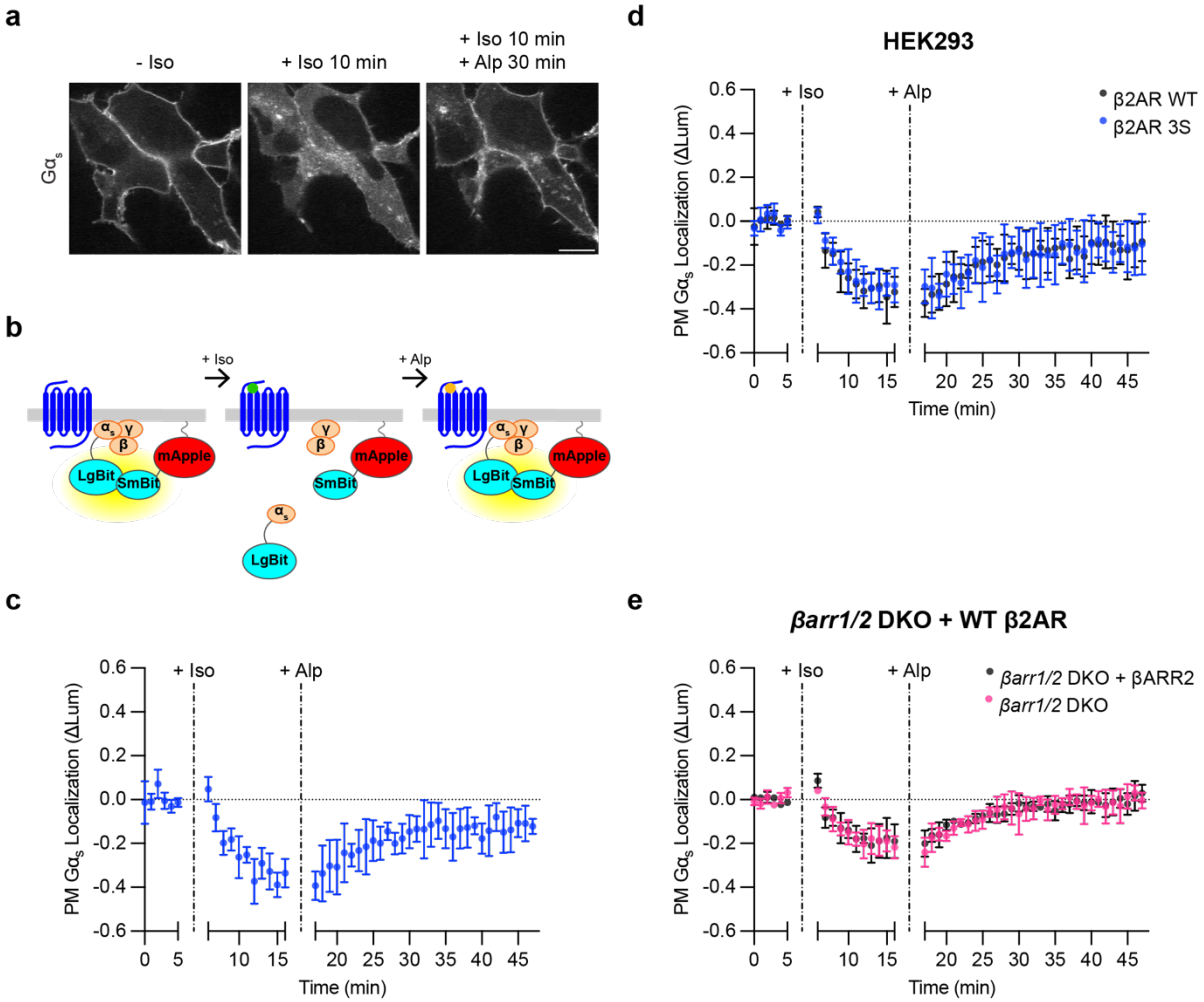


**Figure 2: Redistribution of Gα$_s$ is reversible after receptor inactivation and independent of receptor endocytosis. a)** Representative stills from time-lapse confocal microscopy of live HEK293 cells stably expressing Flag-β2AR and transfected with EGFP-Gα$_s$, myc-Gβ$_1$, and untagged Gγ$_2$ either before drug treatment, after 10 minutes of Iso (100 nM) treatment, or after 10 minutes of Iso followed by 30 minutes of Alprenolol (Alp, 10 μM) treatment. Images are representative of 4 independent experiments. Scale bar = 10 μm. **b)** Schematic of plasma membrane Gα$_s$ NanoBit bystander assay. **c)** NanoBit bystander assay showing plasma membrane localization of Gα$_s$ in HEK293 cells expressing WT Flag-β2AR after Iso (100 nM at 5 minutes) followed by Alp (10 μM at 16 minutes) treatment. **d)** NanoBit bystander assay showing plasma membrane localization of Gα$_s$ after Iso (100 nM at 5 minutes) treatment followed by Alp (10 μM at 16 minutes) treatment in HEK293 cells expressing either Flag-β2AR WT or Flag-β2AR-3S. Significance (n.s.) determined by two-way ANOVA with Sidak's multiple comparisons test (see Supplementary Table 5). **e)** NanoBit bystander assay showing plasma membrane localization of Gα$_s$ after Iso (100 nM at 5 minutes) followed by Alp (10 μM at 16 minutes) treatment in *βarr1/2* DKO HEK293 cells expressing either βARR2-mApple or mApple. Significance (n.s.) determined by repeated measures two-way ANOVA with Sidak's multiple comparisons test (see Supplementary Table 6). Data are shown as mean ± S.D. of at least 3 biological replicates.

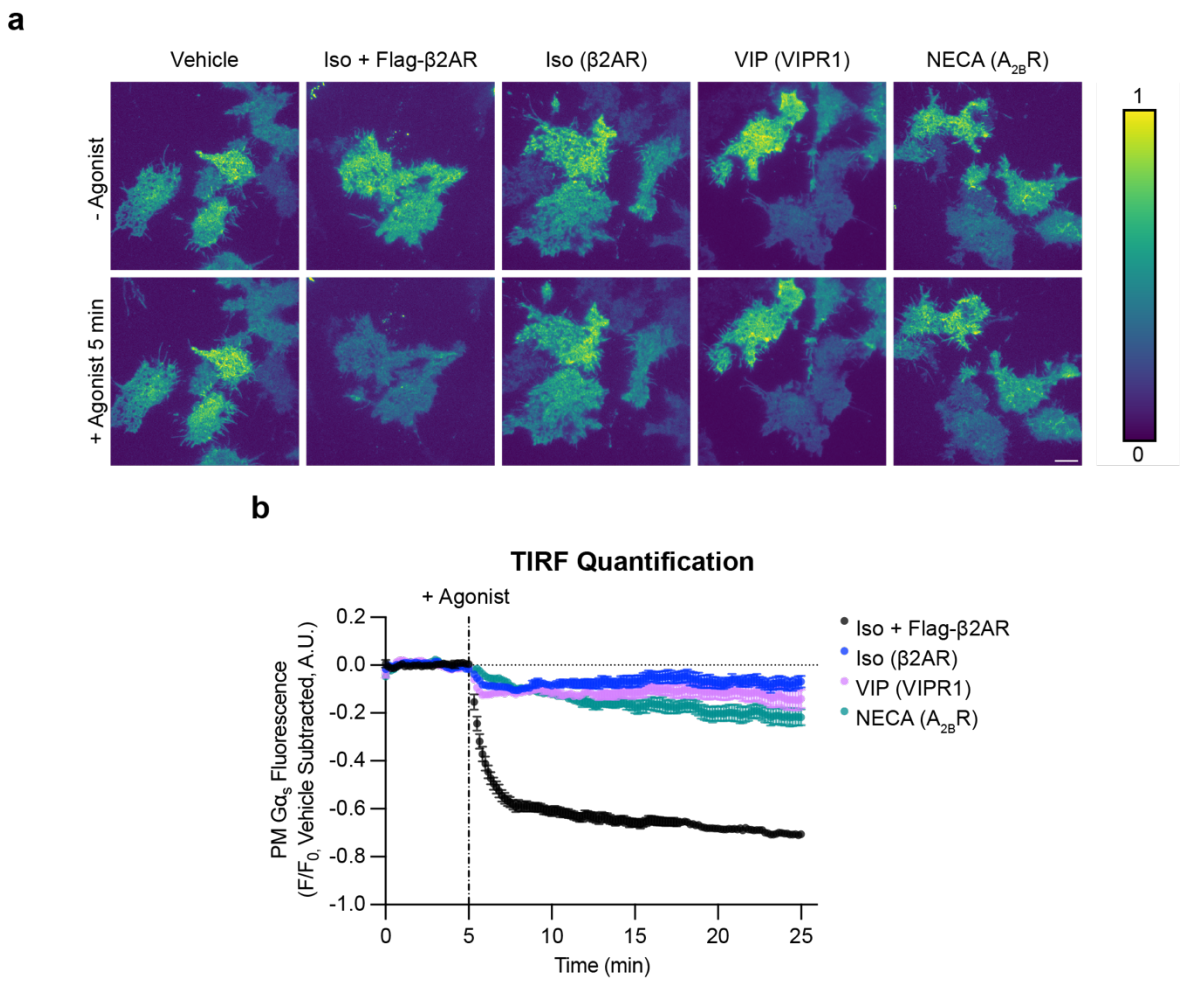


**Figure 3: Activation of 3 endogenously expressed GPCRs drives $G\alpha_s$ redistribution from the plasma membrane. a)** Representative stills from time-lapse TIRF microscopy of $G\alpha_s$ KO1 + EGFP-$G\alpha_s$ rescue cells stably expressing EGFP-$G\alpha_s$ before or after 5 minutes of agonist treatment to activate endogenously expressed GPCRs (β2AR, VIPR1, $A_{2B}R$). Images are shown as heat maps normalized to t = 3 minutes before drug addition for each individual movie. Cells were treated with either vehicle, Iso (1 μM, ± overexpression of Flag-β2AR), VIP (1 μM), or NECA (20 μM). Scale bar = 10 μm. **b)** Quantification of $G\alpha_s$ fluorescence from TIRF movies depicted in a). The average of vehicle control movies (n = 5) at each time point was subtracted before plotting data. n ≥ 4 movies from at least 2 experiments. Data are represented as mean ± S.E.M. of individual movies. Significance determined by repeated measures 2-way ANOVA with Dunnett's multiple comparisons test (see Supplementary Table 8 for p values).

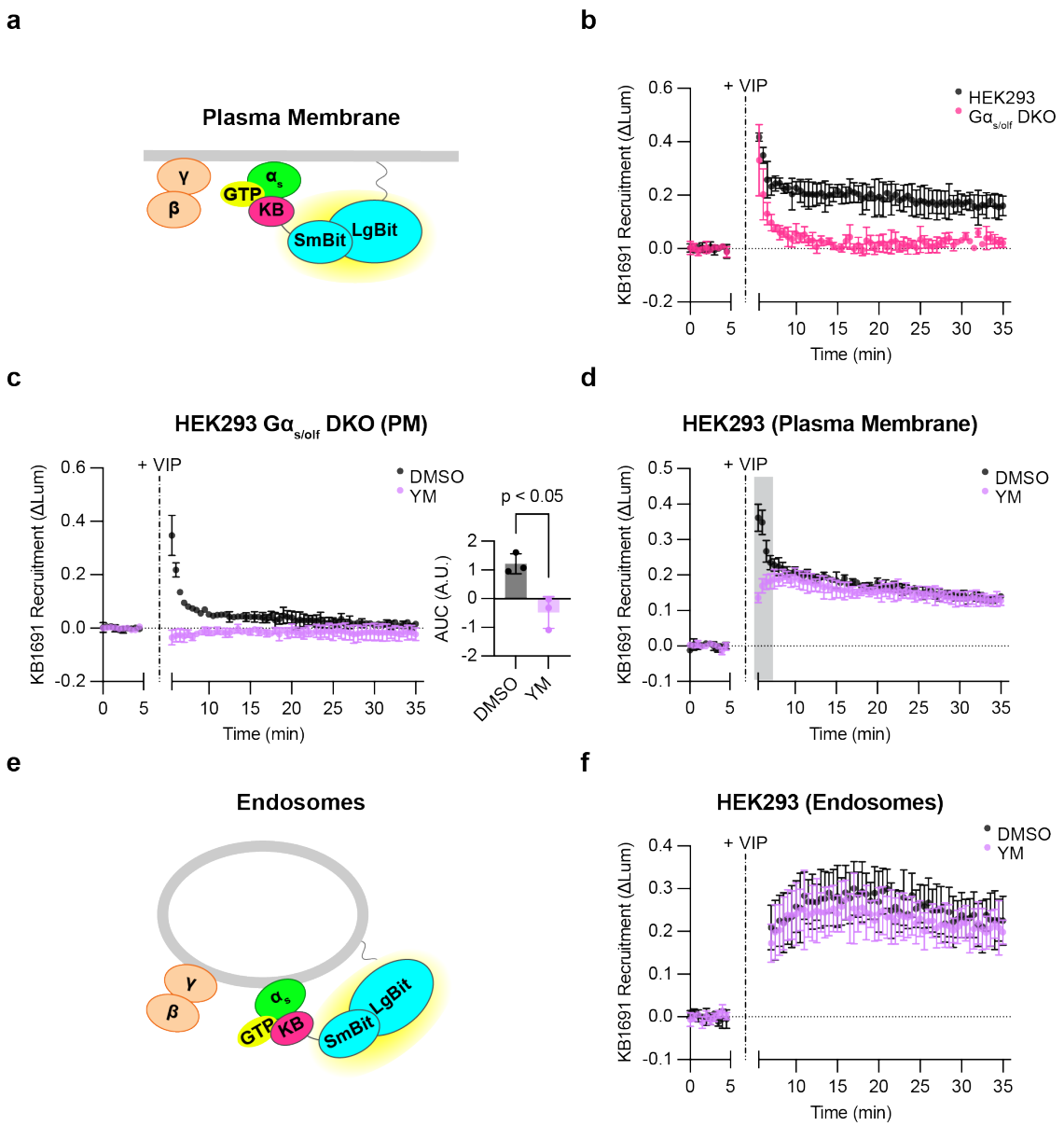


**Figure 4: Detection of active, endogenous G proteins after VIPR1 activation. a)** Schematic of KB1691 (active-state $G\alpha_s$ biosensor) plasma membrane NanoBit bystander assay. **b)** NanoBit bystander assay showing recruitment of KB1691 to the plasma membrane in both HEK293 parental cells and $G\alpha_{s/olf}$ DKO cells expressing Halo-VIPR1. VIP (1 μM) was added after 5 minutes. **c)** Left: NanoBit bystander assay showing recruitment of KB1691 to the plasma membrane in $G\alpha_{s/olf}$ DKO cells expressing Halo-VIPR1 and pretreated with either DMSO (0.1 %) or YM-254890 (1 μM, 30 minutes). Right: AUC of time course. VIP (1 μM) was added after 5 minutes. Significance determined by two-tailed unpaired t test. **d)** NanoBit bystander assay showing recruitment of KB1691 to the plasma membrane in HEK293 cells expressing Halo-VIPR1 and pretreated with either DMSO (0.1 %) or YM-254890 (1 μM, 30 minutes). VIP (1 μM) was added after 5 minutes. Shaded areas represent time points at which the difference between DMSO- and YM- treated cells are statistically significant ($p < 0.05$, determined by repeated measures 2-way ANOVA with Sidak's multiple comparisons test, see Supplementary Table 10). **e)** Schematic of KB1691 endosome NanoBit bystander assay. **f)** NanoBit bystander assay showing recruitment of KB1691 to endosomes in HEK293

cells expressing Halo-VIPR1 and pretreated with either DMSO (0.1 %) or YM-254890 (1 μM, 30 minutes). VIP (1 μM) was added after 5 minutes. Significance (n.s., see Supplementary Table 11) determined by repeated measures 2-way ANOVA with Sidak's multiple comparisons test. Data are shown as mean ± S.D. of at least 3 independent experiments.

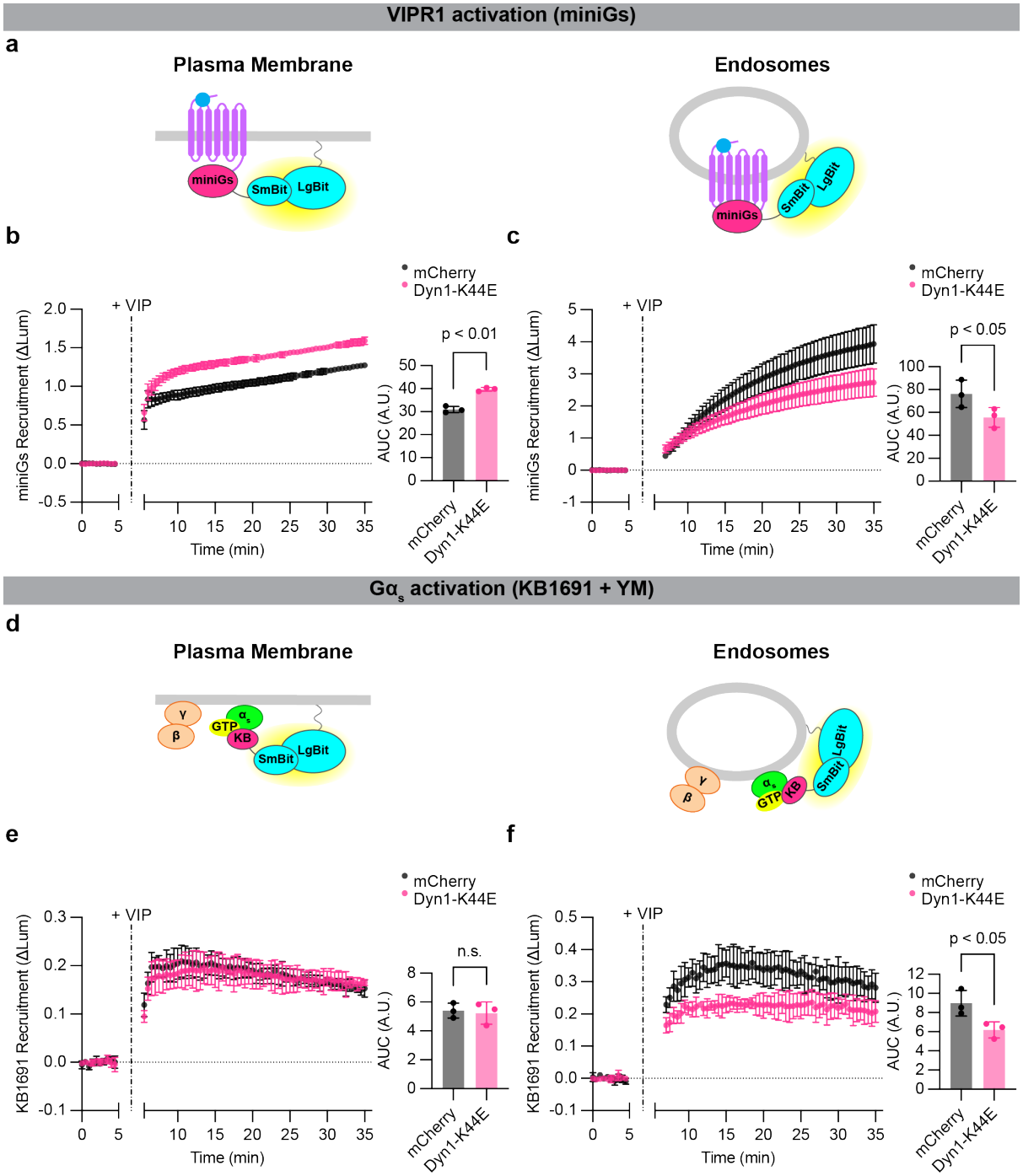


**Figure 5: Active-state Gα$_s$ production on endosomes depends on VIPR1 endocytosis.** **a)** Schematics of mini-Gs (active receptor biosensor) plasma membrane (left) or endosome (right) NanoBit bystander assays. **b,c)** NanoBit bystander assays showing recruitment of mini-Gs to the plasma membrane **(b)** or endosomes **(c)** after activation of Halo-VIPR1 in HEK293 cells transduced with mCherry control or mCherry-Dyn1-K44E BacMam. Left: time course; Right: AUC quantification. VIP (1 μM) was added after 5 minutes. Significance determined by paired two-tailed t-test. **d)** Schematics of KB1691 (active-state Gα$_s$ biosensor) plasma membrane (left) or endosome (right) NanoBit bystander assays. **e,f)** Left: NanoBit bystander assay showing Gα$_s$-specific recruitment of KB1691 to the plasma membrane **(e)** or endosomes **(f)** after activation of Halo-VIPR1 in HEK293 cells transduced with mCherry control or mCherry-Dyn1-K44E BacMam and pretreated with YM-254890 (1 μM, 30

minutes). Right: AUC of time course. VIP (1 μM) was added after 5 minutes. Data for DMSO-treated control cells are shown in Supplementary Figure 8. Significance was determined by repeated measures 2-way ANOVA with Sidak's multiple comparisons test with DMSO control data shown in Supplementary Figure 8 (see Supplementary Table 12). Data are shown as mean ± S.D. of 3 independent experiments.

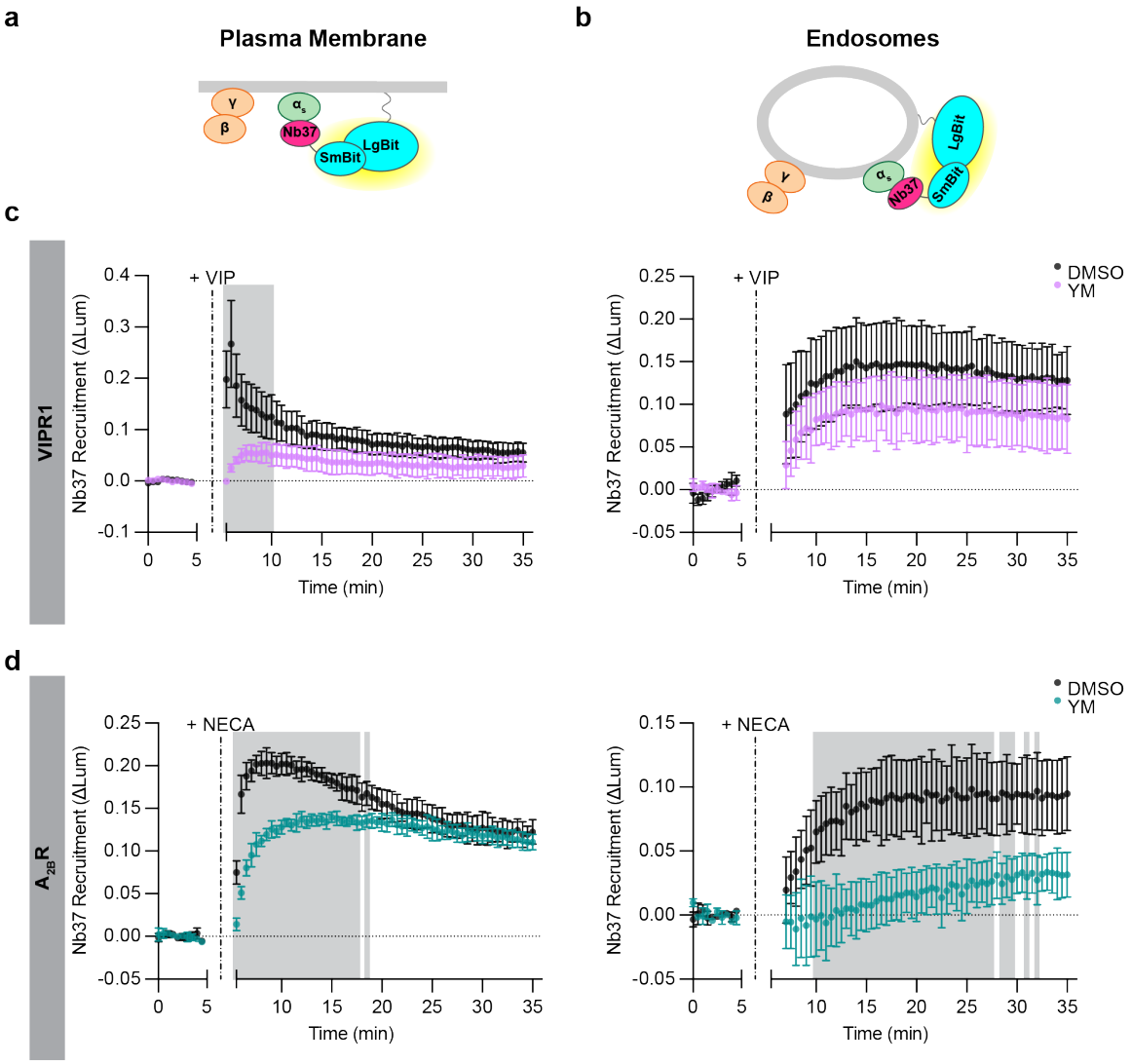


**Figure 6: Differences in endosomal G protein activation by VIPR1 and $A_{2B}R$. a,b)** Schematics of Nb37 (GPCR-G$\alpha_s$ coupling biosensor) plasma membrane **(a)** and endosome **(b)** NanoBit bystander assays. **c)** NanoBit bystander assays depicting Nb37 recruitment to the PM (left) or endosomes (right) after Halo-VIPR1 activation in HEK293 cells pretreated with either DMSO or YM-254890 (1 μM, 30 minutes). Cells were treated with VIP (1 μM) at 5 minutes. **d)** NanoBit bystander assays depicting Nb37 recruitment to the PM (left) or endosomes (right) after Halo-$A_{2B}R$ activation in HEK293 cells pretreated with either DMSO or YM-254890 (1 μM, 30 minutes). Cells were treated with NECA (100 μM) at 5 minutes. Shaded areas in panels c and d represent time points at which the difference between DMSO- and YM- treated cells are statistically significant ($p < 0.05$, determined by repeated measures 2-way ANOVA with Sidak's multiple comparisons test, see Supplementary Tables 13 and 14). Data are shown as mean ± S.D. of at least 3 independent experiments.

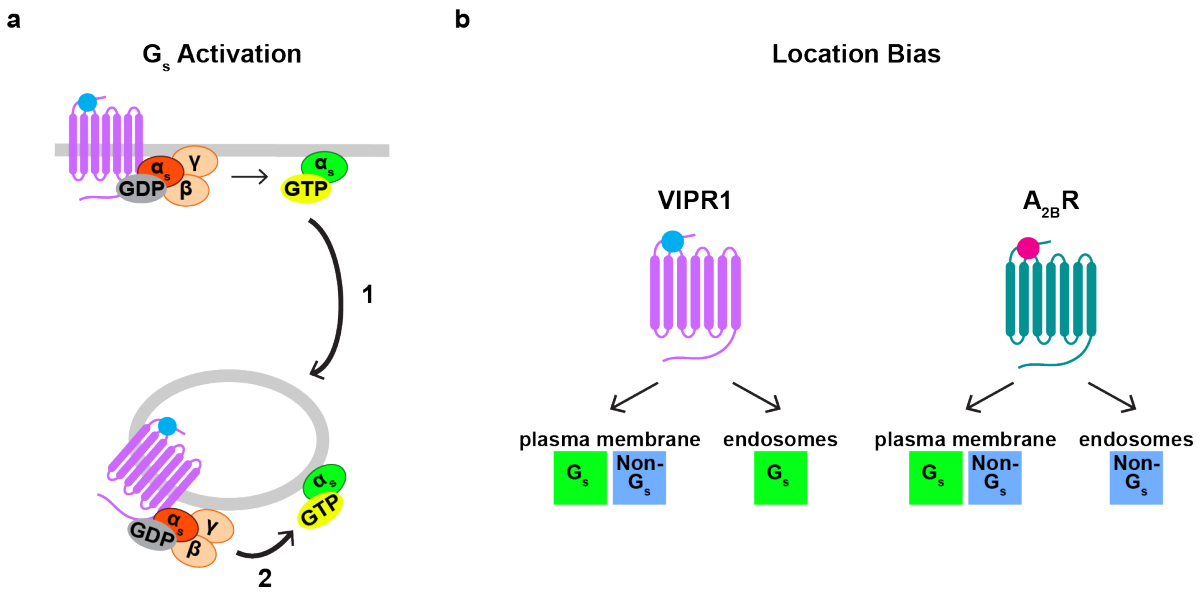


**Figure 7: Proposed models of regulation of endosomal G protein activity. a)** Regulation of endosomal $G\alpha_s$ abundance and activity. Coupling of $G\alpha_s$ to a GPCR at the plasma membrane regulates the abundance of $G\alpha_s$ on endosomes, as it promotes redistribution of $G\alpha_s$ to endosomes independently of GPCR endocytosis (1). A second GPCR-$G\alpha_s$ coupling reaction on endosomes regulates the activity of $G\alpha_s$ on endosomes, which depends on receptor endocytosis (2). **b)** Model of location bias in G protein activation by VIPR1 and $A_{2B}R$. VIPR1 activates both a $G_s$ and non-$G_s$ component of G protein activity on the plasma membrane but preferentially activates the $G_s$ component on endosomes. In contrast, $A_{2B}R$ activates both a $G_s$ and non-$G_s$ component of G protein activity on the plasma membrane but preferentially activates the non-$G_s$ component on endosomes.